Sar1 assembly regulates membrane constriction and ER export

Kimberly R. Long,[1] Yasunori Yamamoto,[1] Adam L. Baker,[1] Simon C. Watkins,[1] Carolyn B. Coyne,[1] James F. Conway,[2] and Meir Aridor[1]

[1]Department of Cell Biology and Physiology and [2]Department of Structural Biology, School of Medicine, University of Pittsburgh, Pittsburgh, PA 15261

The guanosine triphosphatase Sar1 controls the assembly and fission of COPII vesicles. Sar1 utilizes an amphipathic N-terminal helix as a wedge that inserts into outer membrane leaflets to induce vesicle neck constriction and control fission. We hypothesize that Sar1 organizes on membranes to control constriction as observed with fission proteins like dynamin. Sar1 activation led to membrane-dependent oligomerization that transformed giant unilamellar vesicles into small vesicles connected through highly constricted necks. In contrast, membrane tension provided through membrane attachment led to organization of Sar1 in ordered scaffolds that formed rigid, uniformly nonconstricted lipid tubules to suggest that Sar1 organization regulates membrane constriction. Sar1 organization required conserved residues located on a unique C-terminal loop. Mutations in this loop did not affect Sar1 activation or COPII recruitment and enhanced membrane constriction, yet inhibited Sar1 organization and procollagen transport from the endoplasmic reticulum (ER). Sar1 activity was directed to liquid-disordered lipid phases. Thus, lipid-directed and tether-assisted Sar1 organization controls membrane constriction to regulate ER export.

Introduction

Various mechanisms are used by proteins to shape cellular membranes (McMahon and Gallop, 2005). Structurally curved membrane-binding proteins induce membrane tubulation in reactions propagated by membrane-assisted scaffold assemblies (Farsad et al., 2001; Reynwar et al., 2007). Molecular motors bind membranes and attach to the cytoskeleton to pull membrane tubules (Roux et al., 2005). Insertion of amphipathic helixes in membranes induces tubulation by selectively expanding the outer leaflets of bilayers (Bielli et al., 2005; Lee et al., 2005). The morphological nature of intracellular carriers is likely determined by a synergy of all of these mechanisms, although the basis for such synergy is not yet known.

Protein export from the ER is mediated by the cytosolic COPII coat (Lee et al., 2004) that is constructed from two layers. The inner membrane-engaging layer is composed of the small GTPase Sar1 and the protein complexes of Sec23 and Sec24 (Bi et al., 2002). Activation of Sar1 through GTP binding exposes an amphipathic N terminus that embeds in ER membranes, initiating coat recruitment and membrane curvature (Bielli et al., 2005; Lee et al., 2005). The concaved Sec23/24 complex binds activated Sar1 and acidic phospholipids to assemble the inner layer (Matsuoka et al., 1998; Pathre et al., 2003; Blumental-Perry et al., 2006). The outer layer (the Sec13/31 protein complex) is recruited on the inner layer, assembling a 60-nm icosadodecahedral cage through homotypic interactions between Sec31 subunits (Fath et al., 2007; Stagg et al., 2008). Vesicle separation depends on the Sar1 N terminus, which constricts the vesicle neck and proceeds through GTP hydrolysis, controlling fission (Bielli et al., 2005; Lee et al., 2005). Therefore, curved oligomers (Sec23/24) organized by a polymerized cage (Sec13/31) and assisted by an amphipathic

K.R. Long and Y. Yamamoto contributed equally to this paper.

Correspondence to Meir Aridor: aridor@pitt.edu

Y. Yamamoto's present address is Dept. of Physiology and Cell Biology, Kobe University Graduate School of Medicine, Chuo-Ku, Kobe 650-0017, Japan.

Abbreviations used in this paper: ADE, area difference elasticity; AU, arbitrary units; BAR, Bin/Amphiphysin/Rvs; CLSD, cranio lenticulo-sutural dysplasia; DHPE, dihexadecanoyl phosphatidylethanolamine; DOPC, dioleoyl phosphatidylcholine; DOPS, dioleoyl phosphatidylserine; ERES, ER exit site; F-BAR, Fes-CIP4 homology BAR; GUV, giant unilamellar vesicle; Ld, liquid disordered; Lo, liquid ordered; LUV, large unilamellar vesicle; NRK, normal rat kidney; PI4P, phosphatidylinositol 4-phosphate; PLL, poly-L-lysine; tsVSV-G, temperature-sensitive VSV-G; VSV-G, vesicular stomatitis virus glycoprotein; wt, wild type.

The Rockefeller University Press $30.00
J. Cell Biol. Vol. 190 No. 1 115–128
www.jcb.org/cgi/doi/10.1083/jcb.201004132

domain (Sar1) mediate vesicle formation and fission. Purified COPII proteins recapitulate key aspects of vesicle biogenesis on ER membranes or liposomes (Matsuoka et al., 1998).

However, the structure of COPII does not explain coat activities in the constriction of a vesicle neck required for vesicle fission. The flexible architecture of the Sec13/31 cage reduces forces that are generated through assembly (Fath et al., 2007; Stagg et al., 2008). The bent Sec23/24 complex lacks the rigid configuration required for membrane shaping (characterized in Bin/Amphiphysin/Rvs (BAR) domain–containing proteins; Bi et al., 2002). The assembly of COPII on liposomes with Sar1 proteins that lack the N terminus generates shallow, curved membranes that lack constriction (Lee et al., 2005). Although Sar1 concentrations within the assembled COPII cage are below the required concentration for membrane deformation, COPII subunits may cooperate with functional Sar1 to constrict vesicle necks. Alternatively, Sar1 may function independently of COPII to constrict membranes as observed with other fission-controlling proteins such as the GTPase dynamin. In this model, coat-independent organization of Sar1 controls membrane constriction to regulate the timing of fission and vesicle size. In this study, our experiments explore this alternative model of Sar1 function.

Results

Activated Sar1 constricts and tubulates GUVs

Previous visualization of Sar1 activity on small unilamellar vesicles (80–120 nm) by EM required staining and drying (Bielli et al., 2005; Lee et al., 2005). We used giant unilamellar vesicles (GUVs) to examine the role of Sar1 in membrane constriction in solution. GUVs labeled with Texas red–coupled dihexadecanoyl phosphatidylethanolamine (DHPE) were prepared on indium-covered glass electrodes using an electroformation protocol (Mathivet et al., 1996). Fluorescence microscopy showed uniform circular, nondeformed GUVs of 5–20-µm diameter (Fig. 1 A; and Fig. S1, A and B), allowing for direct imaging and analysis in solution. Incubations with $Sar1^{H79G}$ protein (Sar1-GTP; all proteins tested at 5 µM), a constitutively active mutant of Sar1 that cannot hydrolyze GTP, transformed GUVs into tubules (Fig. 1 C and Fig. S1 C). In contrast, $Sar1^{T39N}$ (Sar1-GDP), a mutant deficient in GTP binding, did not deform GUVs (Fig. 1 B; and Fig. S1, A and B; Aridor et al., 1995). A Sar1 protein in which the first nine amino acids of the amphipathic N terminus were removed (Δ9-Sar1) did not deform GUVs (Fig. S1 B). Most of the reactions proceeded to completion with tubules consuming the liposome membranes. This is anticipated because attraction forces between membrane-bound proteins such as Sar1 are enhanced by the developed membrane curvature (Reynwar et al., 2007). However, reaction intermediates showing tubules emanating from circular GUVs were occasionally observed as well as tubule asters, presumably representing complete tubulation that was initiated at multiple sites on the GUV surface (Fig. S1, A and C). Tubules emanating from circular (nonconsumed) GUVs were also preserved under conditions that restricted Sar1 activity (see Fig. 7). Importantly, no tubulation was observed in reactions that did not contain proteins, nor was any tubulation observed in incubations containing Sar1-GDP or Δ9-Sar1 (Fig. 1, A and B; and Fig. S1, A and B). Thus, Sar1 deforms GUVs into tubules in a manner that was dependent on GTP-induced activation and an intact N terminus. Lipid tubules were generally flexible (Fig. 1 C and Fig. S1 C), although a minor yet striking product (~5–16%, depending on incubation conditions; see Membrane attachments regulate Sar1 organization) was rigid lipid tubules (Fig. 1, D and E). A similar tubulation pattern was observed with wild-type (wt) Sar1 (Fig. 1, F and G). Experiments were performed in low-salt buffers, as increased salt concentration inhibited the electroformation of GUVs. However, we observed similar Sar1-induced tubulation of anionic GUVs in physiological buffers containing 125 mM KOAc (Fig. 2, A and B) and in reactions containing GUVs prepared in 0.1 M sucrose with buffers (Fig. S1). Inspection of deformed liposomes using negative-stain EM suggested that flexible tubules were of 30–60-nm diameter with periodic highly constricted membranes shaped like fused vesicles (Fig. 2, D and E).

Organization of a Sar1 coat on the surface of rigid lipid tubules

Oligomerization of Sar1 may be required to induce membrane deformation, and protein oligomerization can be driven by interactions with deformed membranes (Reynwar et al., 2007). Using cross-linking, we previously demonstrated that liposome-bound Sar1 forms high molecular mass complexes (Bielli et al., 2005). Sar1 tended to aggregate in high-salt buffers, and aggregation was visible even in the absence of cross-linking. Sar1 aggregation was reversed when the protein was dialyzed into low-salt buffers (Fig. 1 H). Thus, hydrophobic interactions are likely to contribute to Sar1 aggregation. Sar1 interactions with membranes were analyzed in low-salt buffers in incubations containing GDP or GTP in the presence or absence of large unilamellar vesicles (LUVs) and cross-linking. The reaction was separated into pellet and supernatant by centrifugation and analyzed using Western blots (Fig. 1, I and J). Although some Sar1 tends to precipitate in these reactions, aggregation was not visible under these conditions after SDS-PAGE gel analysis. In contrast, addition of membranes led to the formation of high molecular mass Sar1 species that were stable in the absence of cross-linking. Formation of high molecular mass species was markedly enhanced by the addition of GTP and stabilized by cross-linking (Fig. 1 I). Importantly, residual GTP-dependent Sar1 aggregation was also evident in supernatants of LUV reactions, which might be the result of LUV deformation and rapture (Fig. 1 J and not depicted). Thus, under conditions of membrane deformation, Sar1 oligomerizes in a membrane- and GTP-dependent manner.

Rigid tubules formed by Sar1 remained stable while floating in solution despite motion associated with solution mixing (Fig. 1, D, E, and G). These tubules were reminiscent of ones formed by Sar1 on ER membranes in permeabilized cells (Fig. S4 C; see Fig. 4 D; Aridor et al., 2001). Needle-like tubules with rigid morphology coated with endogenous Sar1 proteins were visible in vivo in coxsackievirus-infected cells (Fig. S2). These tubules were morphologically reminiscent of ones formed

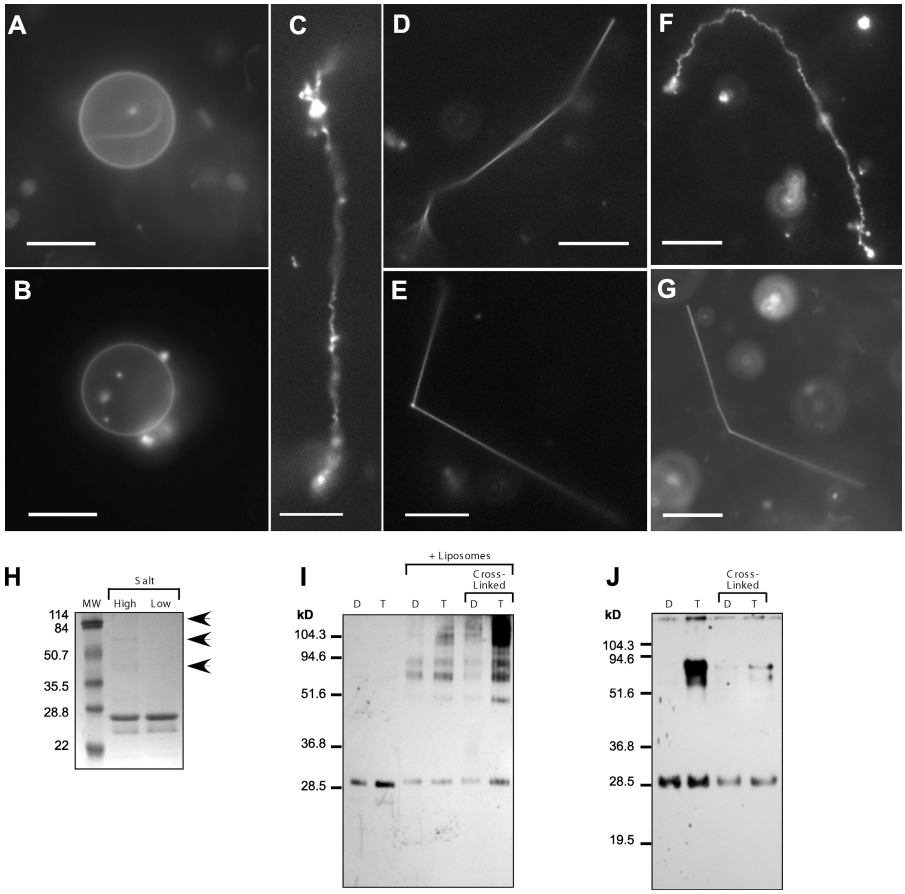

Figure 1. **Sar1 deforms and tubulates GUVs.** (A) GUVs (84.5 mol% DOPC, 5 mol% DOPS, 10 mol% cholesterol, and 0.5 mol% Texas red DHPE) are shown. (B) GUVs incubated with Sar1-GDP in the presence of 2 mM GDP were not tubulated. (C and D) GUVs (as in A) were incubated with Sar1-GTP in the presence of 2 µM BSA, HM buffer (25 mM Hepes-KOH, pH 7.2, and 2.5 mM $Mg(OAc)_2$), 2.5 mM EDTA, and 2 mM GTP for 2 h at 32°C. Sar1 formed flexible (C) and rigid tubules (minor product; D). (E) GUVs incubated with Sar1-GTP in the absence of BSA form flexible (not depicted) and rigid tubules. (F and G) GUVs incubated with wt Sar1 as in E form flexible (F) and rigid (G) tubules. (H) 1 µg Sar1 proteins in high salt (25 mM Hepes-KOH, pH 7.2, 125 mM KOAc, and 1 mM $Mg(OAc)_2$) or low salt (15 mM Hepes-KOH, pH 7.2, 50 mM sorbitol, and 2.5 mM $Mg(OAc)_2$) were analyzed by SDS-PAGE and Coomassie blue staining. Arrows point to high molecular weight (MW) Sar1 proteins. (I and J) 1 µg Sar1 was incubated in the absence or presence of liposomes and 2 mM GDP (D) or GTP (T) as indicated. 100 µM BS^3 cross-linker was subsequently added when indicated. The reactions were fractionated to pellet (I) and supernatant (J) and analyzed by Western blots using Sar1-specific antibodies. Bars, 10 µm.

in GUV–Sar1-containing reactions. The rigid morphology suggested that Sar1 assembly is ordered. Rigid tubules formed by incubations of Sar1-GTP with GUVs that were fixed and extracted with cold methanol were coated with Sar1 proteins (labeled with Sar1 antibodies; Fig. 2 C). Sar1-coated flexible tubules were not detected presumably because of disordered loading that may preclude detection after fixation and labeling. The organization of Sar1 on rigid structures was analyzed by negative-stain EM. A striated pattern (regular banding) was detected on the surface of straight lipid tubules that we infer to represent assembled Sar1 molecules (Fig. 2, F–J). Sar1 organization resembles the appearance of assembled microtubules with a parallel protofilament of Sar1 arranged around the lipid tube (Fig. 2 J; Collins and Vallee, 1987). In some images, periodic striation was evident as bands passing in and out of phase (Fig. 2, H and I), supporting a helical arrangement. In pictures presenting the most compacted configuration, a minimal striation period of 2.47 nm was observed, which is in agreement with the size of a single Sar1 molecule (Fig. 2, H and I; Huang et al., 2001; Stagg et al., 2008). The ordered alignment can explain the rigidity of the tubules. More relaxed configurations have been observed as well (Fig. 2, F and G). Period variability may depend on processing conditions such as staining and dehydration or, importantly, may reflect Sar1 dynamics. We occasionally observed reversal of rigid tubule structures into flexible ones (unpublished data). Importantly, a GFP-tagged Sar1 protein, previously used to study the dynamics of Sar1 interactions with ER exit site (ERES) membranes in vivo (Forster et al., 2006), was capable of deforming GUVs into flexible tubules but did not generate rigid tubules even at high concentrations (≤23 µM; Fig. S3 and not depicted). Presumably, the added GFP tag restricted molecular alignment required for Sar1 organization. As an alternative, we selectively tagged Sar1 with a fluorescent dye at the C terminus (Alexa Fluor 488 Sar1-GTP). This protein formed and coated both rigid and flexible lipid tubules when incubated with GUVs (Fig. S4 D, a–d). Thus, Sar1 can switch between (at least) two assembly states. In ordered configurations, Sar1 generates rigid tubules.

Membrane attachments regulate Sar1 organization

Although many proteins implicated in membrane shaping present lipid-binding specificities, Sar1 binding to ER membranes or liposomes is not lipid specific (Matsuoka et al., 1998; Pathre et al., 2003; Blumental-Perry et al., 2006). Sar1-induced ER tubules failed to elongate in semi-intact cells in the absence of phosphatidic acid or phosphatidylinositol 4-phosphate (PI4P; Pathre et al., 2003; Blumental-Perry et al., 2006). However, GUVs with different lipid compositions, incubated with Sar1-GTP, formed both rigid and flexible tubules, which is in accord with the nondiscriminatory nature of Sar1 membrane binding (Table S1). Specific lipids may kinetically enhance Sar1 assembly as observed with dynamin (Bashkirov et al., 2008). However, these results do not explain the role of specific lipids in

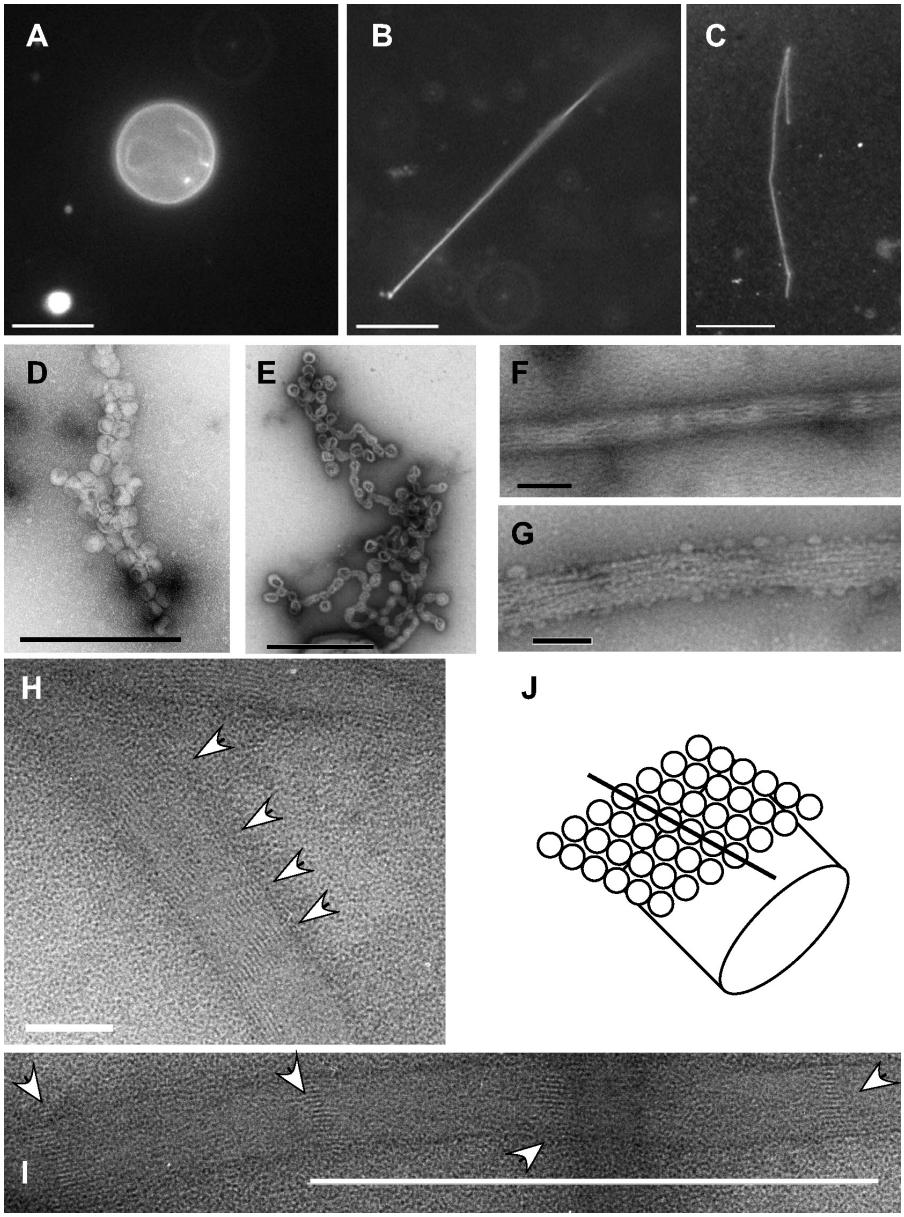

Figure 2. **Formation of a protofilament-like scaffold of Sar1 on lipid tubules.** (A and B) Fluorescent GUVs (54.5 mol% DOPC, 35 mol% DOPS, 10 mol% cholesterol, and 0.5 mol% Texas red DHPE) were incubated without (A) or with (B) Sar1-GTP in a KHM buffer containing 2.5 mM EDTA and 2 mM GTP for 2 h at 32°C and imaged in solution. (C) GUVs (84.5 mol% DOPC, 5 mol% DOPS, 10 mol% cholesterol, and 0.5 mol% Texas red DHPE) were incubated with Sar1-GTP as in Fig. 1, fixed, and analyzed for Sar1 coating using indirect immunofluorescence with anti-Sar1 antibodies. (D and E) Samples prepared as in B were adhered to glow-discharged EM grids and stained with 1% uranyl acetate for imaging by EM. "Beads on a string"–like appearance with vesicle-like structures and constricted vesicle necks suggestive of flexible lipid tubules are shown. (E) 2% paraformaldehyde was added before staining. (F–I) A striated helical-like parallel repeat pattern was detected on rigid-like tubules. Tubulation reactions were performed in the presence (F, H, and I) or absence (G) of 125 mM KOAc. (H and I) Arrowheads point to repeated banding detected on tubule surfaces. (J) A model depicting helical organization of Sar1 on the lipid tube is shown. Open circles represent Sar1 proteins. Bars: (A–C) 10 µm; (D, E, and I) 500 nm; (F and G) 100 nm; (H) 42 nm.

Sar1-induced tubulation of ER membranes. We observed that inclusion of polar lipids in GUV preparations improved the yield of rigid tubule formation (unpublished data). We hypothesize that attachments of the tubulating polar GUVs with the incubation chamber or the air–water interface provide membrane tension that regulates Sar1 organization.

To test this hypothesis, we assembled three reaction chambers to enhance or minimize membrane–surface interactions: uncoated chambers, siliconized chambers, and poly-L-lysine (PLL)–coated chambers (Fig. 3 A). The uncoated chambers were constructed by placing an uncoated cover glass onto an uncoated slide glass (Fig. 3 A). The siliconized and PLL chambers were constructed by placing a siliconized or PLL-coated cover glass, respectively, onto a siliconized slide glass (Fig. 3 A). GUVs were incubated with Sar1-GTP for 1 h in each of the tested chambers. Incubation of Sar1-GTP with GUVs in uncoated chambers led to the formation of flexible tubules and a minor population of rigid tubules, albeit the yield of those was lower than observed in tube reactions (Fig. 3 E). The siliconization of the chamber minimized interactions with the GUVs that now fail to tether to the glass surfaces. Under these conditions, flexible tubules were formed in abundance, whereas the formation of rigid tubules was abolished (Fig. 3, B and E). To confirm that membrane attachments drive the formation of rigid tubules, we used the PLL chamber to provide charge-based binding sites for the phospholipid bilayers. In marked contrast to reactions carried in siliconized chambers, the PLL-coated surface tethered GUVs in a preferential manner, whereas no binding was observed on the opposing siliconized glass surface. Importantly, rigid tubules were now easily detected (Fig. 3, C–E). Rigid tubules anchored on the PLL-coated cover glass or anchored at one end and free at the other were common, suggesting that membrane attachment facilitates the formation of rigid tubules. Flexible tubules were mostly observed unattached in the chamber,

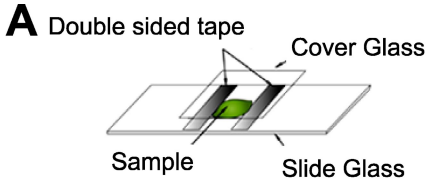

Chamber Type	Cover Glass/Slide Glass
Uncoated chamber	Uncoated /Uncoated
Siliconized chamber	Siliconized /Siliconized
PLL Chamber	Poly-L-Lysine- coated / Siliconized

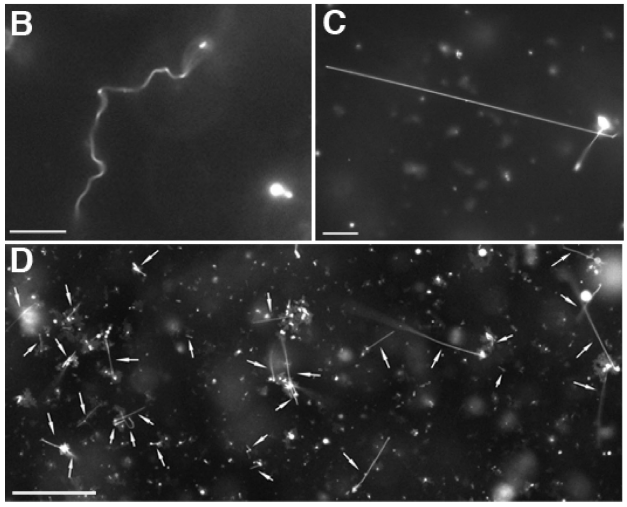

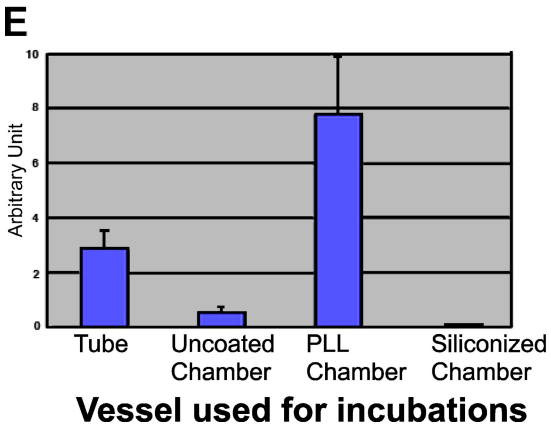

Figure 3. **Membrane attachment controls Sar1 organization.** (A) Schematic representation of reaction chamber assembly. Uncoated chamber was assembled from uncoated cover and slide glasses. Siliconized and PLL chambers were assembled by placing siliconized or PLL-coated cover glasses onto siliconized slide glass. (B) GUVs (84.5 mol% DOPC, 5 mol% DOPS, 10 mol% cholesterol, and 0.5 mol% Texas red DHPE) were incubated with Sar1-GTP in a siliconized chamber for 1 h at 32°C. Flexible tubules were exclusively detected. (C and D) GUVs were incubated with Sar1-GTP in a PLL chamber as in B. The foci of the pictures are taken at the surface of the PLL-coated cover glass. Rigid tubules (D, arrows) were abundant on the PLL-coated glass surface. Images of high and low magnification are shown. (E) Quantification of rigid tubule formation. AU = (mean number of formed rigid tubules/mean number of lipid signals indicative of lipid bilayers before the reaction) × 100 (see Materials and methods). Error bars indicate standard deviation. Bars: (B and C) 10 µm; (D) 50 µm.

although some rigid tubules were also observed in the unattached fraction. Inclusion of acidic lipids in the GUVs enhanced charge-based interactions between GUVs and the PLL chambers and, therefore, rigid tubule formation (10% dioleoyl phosphatidylserine [DOPS]–containing GUVs yielded 13.5 ± 3% rigid tubules; n = 4 experiments; 100 tubules counted per experiment). PLL-coated chambers yielded far more rigid tubules than uncoated chambers or ones formed in tube reactions (Fig. 3 E). Similar results were obtained with wt Sar1 (unpublished data). As observed in tube reactions, GFP-tagged Sar1 could not form rigid tubules under these conditions, although it deformed GUVs into flexible tubules (unpublished data). Thus, rather than simple PLL-supported concentration or aggregation of Sar1 on lipid tubules, correct organization and alignment of Sar1 is required to support rigid tubule formation on tethered membranes.

A role for the Ω loop in Sar1 organization

The conserved N-terminal GTPase domain of Sar1, including switch 1, switch 2, and the β2–β3-connecting loop, provides a wide interaction surface with the GTPase-activating protein complex of Sec23 and Sec31 (Fig. 4 A). A unique C-terminal loop (Ω loop; residues 156–171 in hamster Sar1a) of Sar1 is appended to the GTPase domain (Fig. 4 A), yet the function of this domain is unknown (Huang et al., 2001). The unstructured loop is visible in the crystal structure both in the GDP- and GTP-bound forms and presents a high B value to suggest that it is a dynamic element of Sar1 that can function in protein–protein or protein–lipid interactions. Importantly, the loop does not contact COPII in the assembled cage (Fig. 4 A), yet a mutation in a conserved residue within the loop (T158A) inhibits the ability of the protein to drive vesicle formation from microsomes in incubations containing purified COPII proteins (Huang et al., 2001). The loop may participate in Sar1 organization during membrane constriction. Substitutions within the loop should not affect the ability of the protein to recruit and nucleate COPII at ERES or to tubulate membranes, leading to the formation of highly constricted flexible tubules, yet may inhibit scaffold assembly as reported by rigid tubule formation.

To address these hypotheses, we replaced a conserved sequence within the loop (156-QTTG-159) with alanine residues (Sar1^{QTTG}) in Sar1 wt or Sar1-GTP background (H79G) and produced recombinant proteins for analysis. We used established assays that report the Sar1- and GTP-dependent recruitment and nucleation of COPII at ERES (Shimoi et al., 2005; Aridor and Fish, 2009). To analyze the membrane recruitment of the inner coat, ER microsomes were incubated with cytosol and increasing concentrations of Sar1^{QTTG}-GTP. Subsequently, the membranes were washed and probed for Sec23 recruitment using Western blotting. Sar1^{QTTG}-GTP effectively recruited Sec23 to membranes, as did Sar1-GTP (Fig. 4 B). Morphological analysis was used to follow Sar1-dependent nucleation of the outer layer COPII cage at defined ERES. Normal rat kidney (NRK) cells were permeabilized and incubated with cytosol and Sar1-GTP or Sar1^{QTTG}-GTP, and the assembly of Sec13 was analyzed by indirect immunofluorescence. In agreement with the effective recruitment of Sec23 to microsomes, Sar1^{QTTG}-GTP

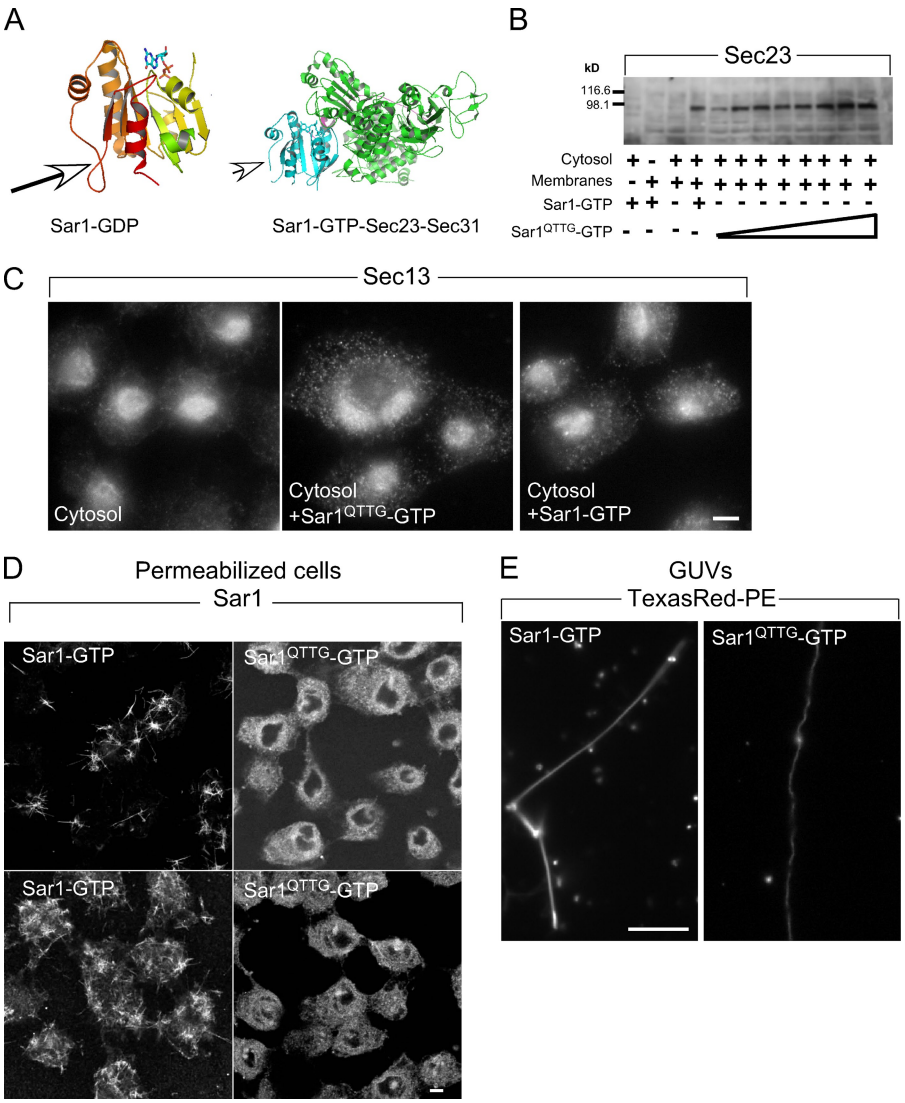

Figure 4. **The Ω loop is required for Sar1-induced rigid tubule formation.** (A) The structure of hamster Sar1a bound to GDP (Huang et al., 2001) and GTP-bound Sar1 assembled with Sec23 and Sec31 (Bi et al., 2007). Arrows point to the Ω loop. (B) Sar1^{QTTG}-GTP recruits Sec23/24. NRK membranes were incubated with cytosol in the presence of 1 µg Sar1-GTP or increasing concentrations (0.1–2 µg/60 µl) of Sar1^{QTTG}-GTP as indicated, washed, and Sec23/24 recruitment was determined by Western blotting with a Sec23-specific antibody. The first lane shows control incubation with Sar1-GTP, cytosol, and no membranes. (C) Sar1^{QTTG}-GTP recruits Sec13/31. NRK cells were permeabilized and incubated with cytosol and 2 µg/220 µl Sar1-GTP or Sar1^{QTTG}-GTP for 30 min at 32°C. The distribution of Sec13/31 was determined by indirect immunofluorescence using a Sec13-specific antibody. Note the punctate localization of recruited Sec13 at ERES. (D and E) Sar1^{QTTG}-GTP does not generate rigid tubules. (D) NRK cells were permeabilized and incubated without cytosol in the presence of 2 (top) or 20 µg (bottom; 220 µl final volume) Sar1-GTP or Sar1^{QTTG}-GTP as indicated. The distribution of Sar1 was determined by indirect immunofluorescence. (E) GUVs (as in Fig. 3) were incubated with 5 µM Sar1-GTP or Sar1^{QTTG}-GTP. Tubules were visualized in solution using Texas red DHPE (PE). Bars: (C and D) 5 µm; (E) 10 µm.

induced efficient recruitment and nucleation of the coat outer layer at defined punctated ERES as observed with Sar1-GTP (Fig. 4 C). Therefore, Sar1 activation and COPII recruitment activities were well preserved in the QTTG to AAAA substitution mutant protein. Importantly, a Sar1^{QTTG} mutant protein that is not blocked in GTP hydrolysis (Sar1^{QTTG} wt) did not support recruitment of COPII to membranes (unpublished data). Therefore, inhibition of GTP hydrolysis by the H79G mutation was required for Sar1^{QTTG} to mediate stable COPII assembly, suggesting that the GTPase activity of Sar1^{QTTG} is functional (unpublished data).

Although Sar1^{QTTG}-GTP was fully functional in COPII recruitment and nucleation, it was inactive in forming rigid tubules. Sar1 tubulation activity was first tested on ER membranes in semi-intact cells, NRK cells incubated with Sar1-GTP, or Sar1^{QTTG} -GTP in the absence of COPII components (Fig. 4 D and Fig. S4 C; Aridor et al., 2001). Under these conditions, Sar1 generates numerous cargo-selective uniform and nonconstricted (40–50 nm) rigid tubules on ER membranes (Aridor et al., 2001). Although Sar1-GTP formed numerous rigid tubules, incubations with Sar1^{QTTG}-GTP did not generate any visible Sar1-coated tubules even when tested at high concentrations (Fig. 4 D). Thus, the QTTG to AAAA substitution inhibited the ordered organization of Sar1 on membranes. To test this possibility directly, we followed the formation of Sar1-induced rigid lipid tubules on fluorescent GUVs. The experiments were performed in PLL-coated chambers to maximize membrane attachment and, thus, rigid tubule formation. However, unlike Sar1-GTP, Sar1^{QTTG}-GTP protein failed to form rigid lipid tubules (Fig. 4 E; and Fig. S1, A and D). Importantly, Sar1^{QTTG}-GTP generated flexible tubules (Fig. 4 E; and Fig. S1, A and D). wt Sar1 is similarly functional in forming Sar1-coated rigid tubules on ERES and GUVs (Fig. 1; Aridor et al., 2001). However, wt Sar1^{QTTG} was also incapable of organizing on membranes and forming rigid tubules as observed with Sar1^{QTTG}-GTP (unpublished data).

We used small liposomes (LUVs; 150–300 nm) and EM analysis to monitor membrane constriction by Sar1 proteins. Sar1-GTP generated highly uniform cylinder-like smooth tubules with a constant diameter of ~22 nm (Fig. 5 A). Although not as notable as on tubules formed from GUVs, periodic striations were evident (Fig. 5 A, arrows). The uniform morphology

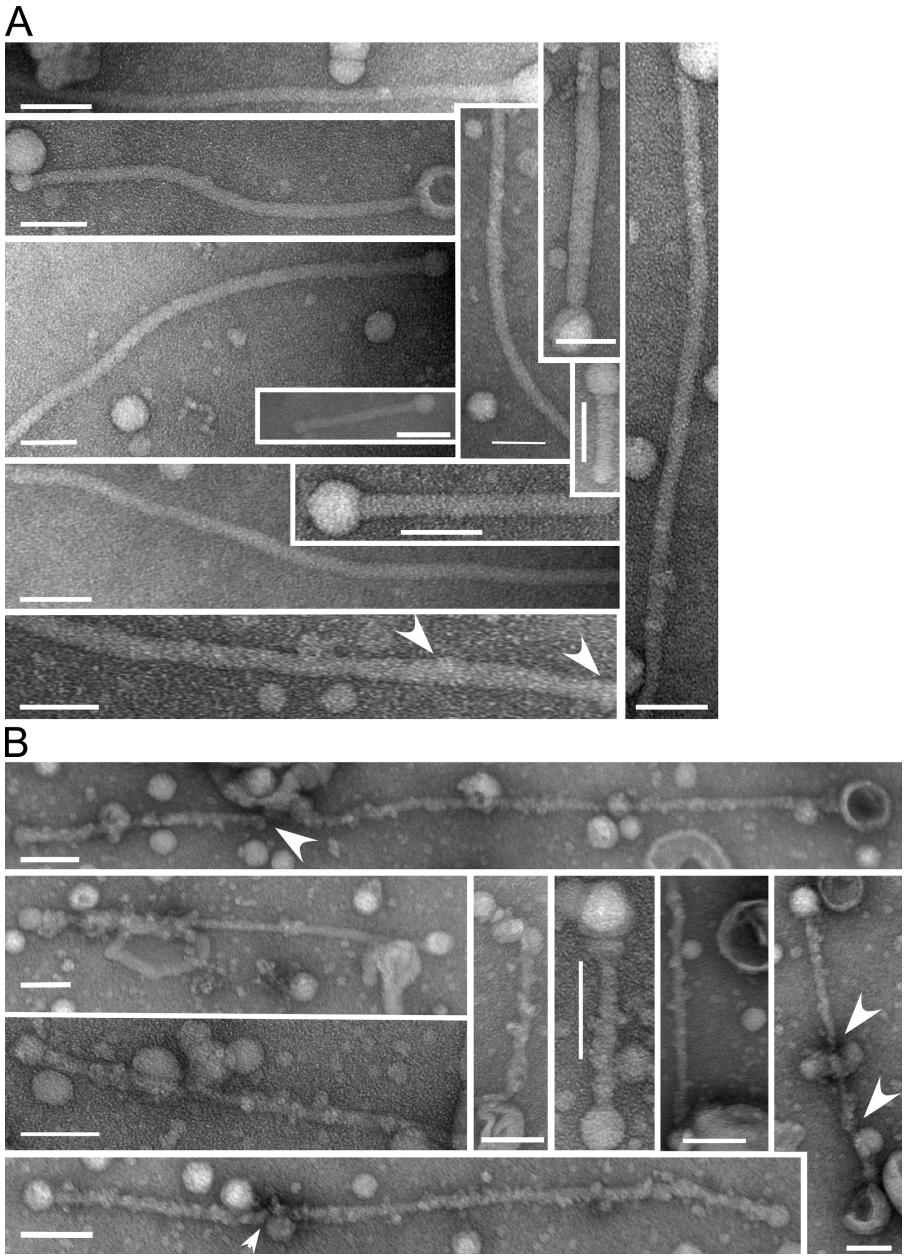

Figure 5. **Sar1-GTP proteins tubulate LUVs.** (A and B) LUVs composed of 20 mol% cholesterol, 75 mol% DOPC, and 5 mol% DLPA were prepared as described previously (Bielli et al., 2005) with the following modification. Lipids were rehydrated in a buffer containing 25 mM Hepes-KOH, pH 7.2, 1 mM $Mg(OAc)_2$, and 50 mM sorbitol for 1 h at 37°C. LUVs were sized by repetitive extrusion through a polycarbonate filter (400-nm pores; Avanti Polar Lipids, Inc.). Resulting LUVs (150–300-nm diameter) were incubated with 5 µM of either Sar1-GTP (A) or $Sar1^{QTTG}$-GTP (B) for 2 h at 32°C in a KHM buffer containing 2.5 mM EDTA, 2.5 mM $Mg(OAc)_2$, and 2 mM GTP. Samples were adhered to glow-discharged EM grids and stained with 1% uranyl acetate for EM analysis. Note the uniform appearance of tubules generated by Sar1-GTP (A) and the irregular morphology of tubules generated by $Sar1^{QTTG}$-GTP (B). Arrowheads indicate a repetitive banding pattern (A) and areas of increased membrane constriction (B). Bars, 100 nm.

suggests that Sar1 scaffolds assembled on LUVs. In contrast, the $Sar1^{QTTG}$-GTP mutant generated highly irregular tubules with numerous membrane constrictions (Fig. 5 B, arrows). The analysis of GUVs and LUVs suggests that $Sar1^{QTTG}$ is highly effective in constricting membranes. In agreement, the protein assembled high molecular mass complexes on membranes when analyzed by cross-linking (Fig. S5). However, $Sar1^{QTTG}$ is deficient in rigid tubule formation or the control of membrane constriction, deficiencies that are likely derived from an inability to organize on membranes.

Sar1 organization regulates ER export

To begin exploring the physiological role of Sar1 organization, we followed the effect of $Sar1^{QTTG}$ expression on the synchronized mobilization of two cargo proteins from the ER: (1) the GFP-tagged temperature-sensitive vesicular stomatitis virus glycoprotein (tsVSV-G; tsVSV-G–GFP), which aggregates in the ER at a nonpermissive temperature (40°C) yet trimerizes upon a temperature shift to a permissive temperature (32°C) and captured in 60–80-nm COPII-coated vesicles for ER exit (de Silva et al., 1990; Bielli et al., 2005), and (2) procollagen, the assembly of which requires the addition of ascorbate (Starkuviene and Pepperkok, 2007). In the absence of ascorbate, the unassembled protein is retained in the ER. Upon ascorbate addition, hydroxylation enables procollagen assembly in a triple-helical rod-like configuration (300 nm in size) for ER exit. Unlike VSV-G, assembled procollagen does not fit in conventional COPII vesicles, yet the export of procollagen from the ER is COPII dependent (Fig. 6 C; Mironov et al., 2003).

We examined the QTTG substitution in Sar1 wt background because the H79G mutation (Sar1-GTP) inhibits vesicle fission (Bielli et al., 2005). tsVSV-G–GFP and procollagen-expressing

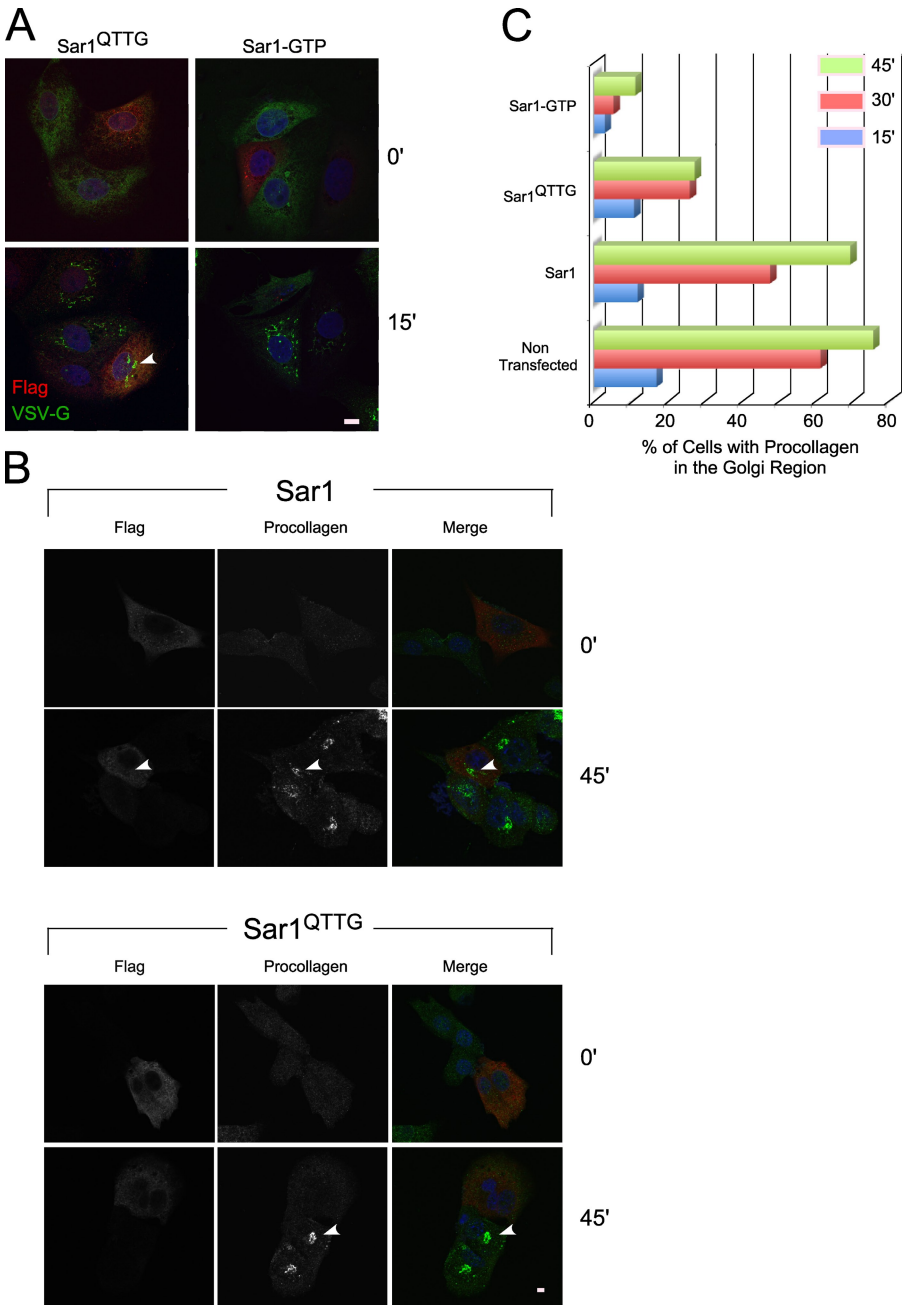

Figure 6. **Expression of Sar1^{QTTG} inhibits the traffic of procollagen from the ER to the Golgi.** (A) MDCK cells expressing tsVSV-G–GFP (stable Tet-off expression) were transfected with Flag-Sar1^{QTTG} or Flag-Sar1-GTP as indicated. Tetracycline was removed, and cells were incubated at 40°C to accumulate tsVSV-G–GFP in the ER. Cells were shifted to 32°C for 15 min. The expression of Flag-Sar1 (red) and the localization of tsVSV-G–GFP (green) were determined using indirect immunofluorescence. The arrowhead indicates arrival and concentration of tsVSV-G–GFP at the Golgi in a Flag-Sar1^{QTTG}–expressing cell. (B) NIH3T3 cells were transiently transfected with Flag-Sar1 proteins as indicated. The cells were treated with ascorbate to induce the ER export of procollagen for the indicated time. The expression of Sar1 proteins and the localization of endogenous procollagen type I were determined by indirect immunofluorescence. Arrowheads indicate arrival and concentration of procollagen at the Golgi in a Flag-Sar1–expressing cell (top) or nontransfected cell (bottom) located next to cells expressing Flag-Sar1^{QTTG} where transport is not observed. (C) Bar graphs represent quantification of the arrival and concentration of procollagen at the Golgi region in cells expressing Sar1a proteins (Sar1 wt, Sar1^{QTTG}, Sar1-GTP, or nontransfected cells) at the indicated times after ascorbate addition, conducted on three independent experiments where each expression group (134–723 cells/group/time point) was pooled and analyzed in a cumulative manner. To estimate the variability between experiments, we independently requantified the 45-min time point for individual experiments comparing traffic of procollagen in cells expressing Sar1 wt (total of 325 cells) to traffic in cells expressing Sar1^{QTTG} (423 cells) or Sar1-GTP (222 cells). Sar1^{QTTG} and Sar1-GTP inhibited procollagen traffic by 57.37 ± 3.83% and 86.63 ± 0.75% (SEM; n = 3 experiments), respectively, compared with Sar1 wt, which is in agreement with cumulative analysis (60.75% and 83.9%, respectively). Bars, 5 µm.

cells were transfected with constructs expressing Sar1 proteins for analysis. Expression of Sar1-GTP (Fig. 6 A) or Sar1^{QTTG}-GTP (not depicted) blocked export of tsVSV-G–GFP from the ER and delivery to the Golgi complex. However, expression of Sar1^{QTTG} did not affect the arrival of tsVSV-G–GFP to the Golgi nor did we detect any kinetic delays in tsVSV-G–GFP traffic (Fig. 6 A and not depicted). Therefore, Sar1^{QTTG} is not an effective trans–dominant-negative inhibitor of VSV-G export from the ER. In contrast, the mobilization of procollagen from the ER to the Golgi was markedly inhibited by the expression of Sar1^{QTTG}. In the majority of transfected cells, we could not detect effective arrival of procollagen to the Golgi region throughout a time course of procollagen transport (Fig. 6, B and C). We quantified the arrival of procollagen in the Golgi after ascorbate addition (Fig. 6 C). Similar to nontransfected cells, overexpression of wt Sar1 did not affect the arrival of procollagen at the Golgi (8% inhibition when compared with nontransfected cells at peak accumulation of procollagen in the Golgi). Expression of Sar1-GTP led to robust inhibition with only 12% of the cells showing procollagen concentration in the Golgi region at 45 min after the initiation of ER exit (85% inhibition; Fig. 6, B and C). Importantly, expression of Sar1^{QTTG} inhibited the transport of procollagen to the Golgi with only 25% of the cells showing concentration of procollagen at the Golgi region (65% inhibition at the 45-min time point; Fig. 6, B and C). Sar1^{QTTG} is fully functional in known activities of the wt protein, yet it is deficient in scaffold assembly and regulated membrane constriction (Fig. 4, D and E; Fig. 5 B; and Fig. S1, A and D). Therefore, Sar1 organization and regulated membrane constriction may play a key role in procollagen exit from the ER.

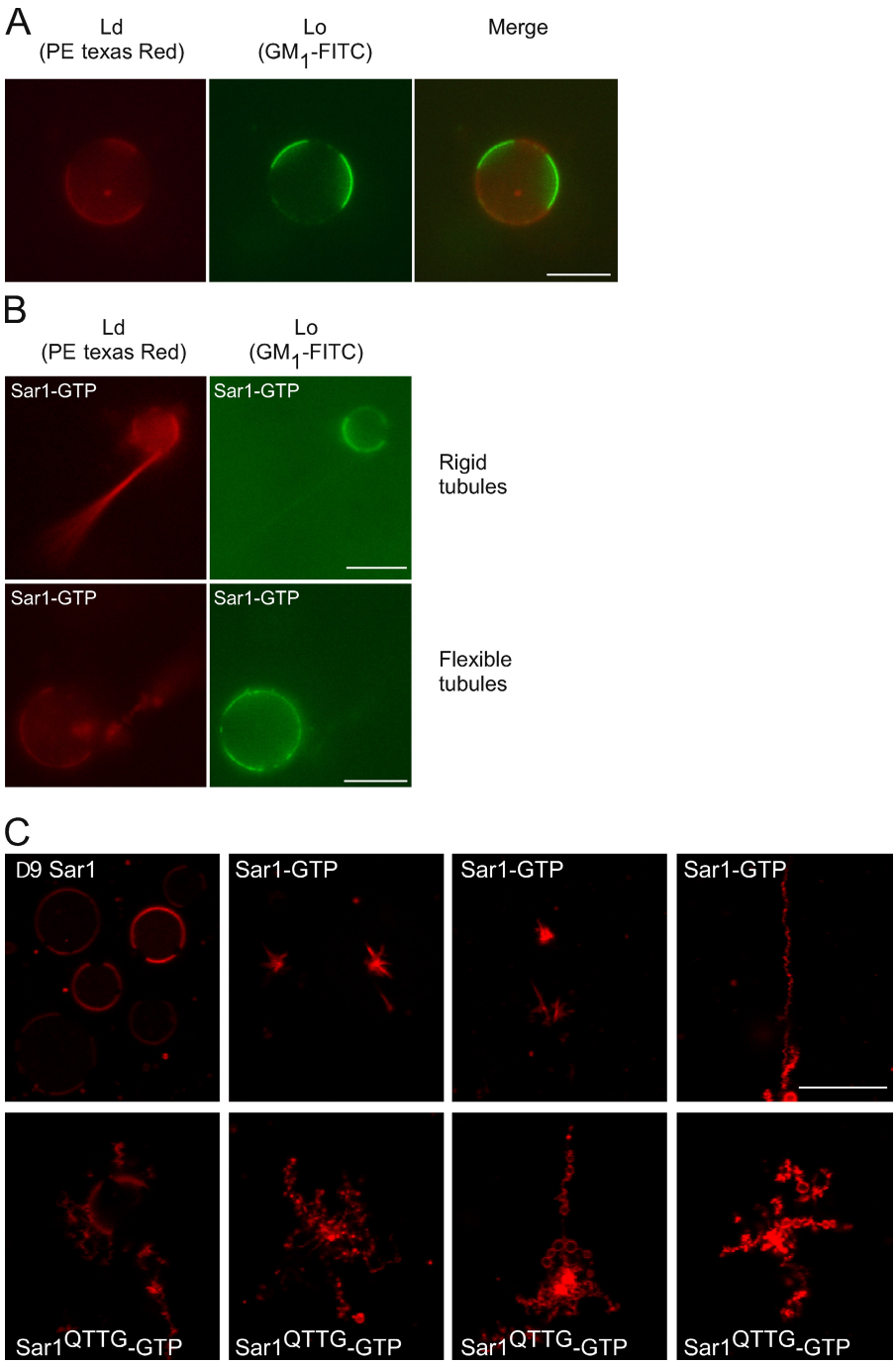

Figure 7. **Sar1 activity is directed to Ld phases.** (A) GUVs composed of DOPC/cholesterol/brain sphingomyelin (3:1:3) supplemented with 1% DOPS, 1% GM1, and 0.5% Texas red DHPE (PE) were electroformed in 25 mM Hepes-KOH, pH 7.2, at 65°C. The Lo phase was labeled with 2.5 µg/ml FITC-tagged cholera toxin B subunit (Lo probe). Texas red DHPE is incorporated in the Ld phase. (B) 20 ng/µl GUVs were reacted with 5 µM Sar1-GTP in the presence of 2.5 µg/ml FITC cholera toxin B subunit for 2 h at 27°C or RT in a PLL chamber (see Materials and methods). (C) 5 µM Δ9Sar1, Sar1-GTP, or Sar1^{QTTG}-GTP was incubated as in B without the Lo probe in reactions containing GUVs produced in sucrose buffers, and tubulation morphology was analyzed. (B) Note that phase-separated GUVs inhibited Sar1 tubulation activity. Sar1 preferentially constricted Ld phase into flexible and rigid tubules. (C) Note that distinct tubular morphologies were observed with Sar1^{QTTG}-GTP. Bars, 10 µm.

Lipid microdomains regulate Sar1 activity

We examined how Sar1 activities are modulated by lipid composition and organization. We analyzed GUVs composed of dioleoyl phosphatidylcholine (DOPC), cholesterol, and brain sphingomyelin (3:1:3 ratio), as these GUVs presented clear separation between lipid phases (liquid-disordered [Ld] and -ordered [Lo] phases; Fig. 7 A; Roux et al., 2005) and are suitable for morphological analysis. The Ld phase was identified by the distribution of 0.5 mol% Texas red DHPE, and the Lo phase was detected by the binding of FITC-labeled B subunit of cholera toxin to GM1 (incorporated in GUVs at 0.1 mol%) that partitions exclusively in Lo phases under these conditions. Partitioned GUVs mostly inhibited Sar1-induced tubulation, and residual tubulation activity was observed extending from largely preserved circular GUVs (Fig. 7 B). Thus, Lo phases inhibit the constrictive activity of Sar1. Omission of the B subunit of cholera toxin gave the same results (unpublished data). Importantly, the tubulation activity of Sar1 was exclusively directed to the Ld phase (Fig. 7 B), whereas the Lo phases remained in spherical unperturbed portions of the GUV. The preferential activity of Sar1 on Ld phases and inhibition of membrane constriction by Lo phases suggest that the membrane constriction activity is controlled by lipid composition, whereas microorganization of lipids in membranes spatially directs Sar1 membrane–deforming

activities. Interestingly, incubation of phase-partitioned GUVs with Sar1^{QTTG}-GTP in PLL chambers led to distinct vesiculation-like morphology with an increased number of small lipid particles (Fig. 7 C). Future studies should examine whether membranes with reduced elasticity that are phase partitioned promote fission under conditions of disordered or concentrated Sar1 loading.

Discussion

We examined the hypothesis that Sar1, the small GTPase that supports COPII vesicle fission, organizes on membranes in a coat-independent manner to constrict membranes. Our results suggest that regulated scaffold assembly by Sar1, which is similarly observed with other membrane shaping and fission proteins, provides a unifying mechanism used to control membrane constriction for fission events.

Scaffold assembly in membrane shaping

Sar1-organized assembly is likely revealed by the highly rigid morphology of Sar1-coated tubules floating in solution that are formed in defined minimal reactions containing Sar1 and GUVs (Fig. 1), the rigid Sar1-induced tubulation at ERES in permeabilized cells (Fig. 4 and Fig. S4), and perhaps by the morphologically similar needle-like tubules coated with endogenous Sar1 in coxsackievirus-infected cells (Fig. S2). EM analysis indicated that Sar1 forms an ordered scaffold that is reminiscent of helical protofilament assemblies previously observed with microtubules (Fig. 2 and Fig. 5). The structural details of the Sar1 scaffold remain to be explored. Although in vitro tubulation reactions lead to the formation of exaggerated intermediates, such analysis suggests that scaffold assembly is a common mechanism used for membrane bending. For example, a dense collar of dynamin coats membranes to drive tubulation and fission (Bashkirov et al., 2008; Pucadyil and Schmid, 2008), and the self-assembly of the Fes-CIP4 homology BAR (F-BAR) domain in helical scaffolds promotes the formation of uniform nonconstricted tubules (Frost et al., 2008). What is the role of scaffold assembly in membrane deformation? Our EM analysis on tubules formed using GUVs (Fig. 2) or LUVs (Fig. 5) suggests that one role is to control and limit membrane constriction. Tubules derived from GUVs yielded both rigid and flexible tubules. By EM, we observed wide (>40-nm diameter) uniform nonconstricted tubules, likely corresponding to rigid tubules, and "bead on a string"–like morphology consisting of vesicles connected by constricted necks, most likely corresponding to flexible ones (Fig. 2). Sar1 also generated highly uniform tubules on LUVs (22-nm diameter; Fig. 5). The Sar1^{QTTG} mutant was not capable of forming rigid tubules from GUVs or ER membranes (Fig. 4) and generated tubules with irregularities and areas of local constrictions on LUVs (Fig. 5). Thus, organized assembly of Sar1 correlated with lack of constriction. Recent EM studies on the F-BAR domains of pacsin support this conclusion. The domain forms uniform nonconstricted tubules (>40 nm) coated with a regular striated helical pattern reminiscent of a rigid scaffold, narrow yet uniform tubules, and highly constricted, vesiculated ones with "beads on a string"–like morphology (Wang et al., 2009), all similar to morphologies observed with Sar1. As with Sar1, the regulation of pacsin assembly and membrane constriction is attributed to a short, unstructured loop that is unique to this F-BAR domain. Although the Sar1 and pacsin unstructured loops differ in their chemical nature (with the pacsin loop being more amphipathic to support membrane binding), alterations in membrane placement regulated by unstructured loops may be similarly used to control membrane constriction. In Sar1, the Ω loop, which is located at the edge of the β sheet core (Fig. 4), may provide a Sar1–Sar1 contact site or contact phospholipids to define Sar1 placement. Both the analogy to pacsin and our cross-linking experiments (Fig. 1 and Fig. S5) support the former possibility, yet, unlike pacsin, the Ω loop of Sar1 is not required for membrane binding. GTP-bound Sar1^{QTTG} interacts with both liposomes and ER membranes effectively and recruits COPII to ER membranes (Fig. 4 and Fig. 5). This is expected, as Sar1 proteins use the extended amphipathic N terminus for membrane binding.

Area difference elasticity (ADE) as a model for membrane constriction and fission

Sar1-supported membrane constriction and fission are driven by the selective expansion of the membrane outer leaflet that is induced by the membrane insertion of the N terminus (Bielli et al., 2005). Under conditions of constant volume and tension, the increased area difference between the membrane leaflets generates elastic stress in the inner leaflet that is accommodated by shape changes. The ADE model predicts that GUVs will transform from spheres to cylinders, and upon further expansion of the outer leaflet, will change into beads on a string-like vesiculated morphology (Inaoka and Yamazaki, 2007). These changes, which are observed with Sar1 (Figs. 1–3), minimize the energy derived from elastic stress. Therefore, it is reasonable to assume that the morphological tubulation outcomes observed with Sar1 are indicative of local concentrations of Sar1 N termini in membranes. Sar1^{QTTG} exclusively formed vesiculated (flexible) tubules to indicate that it is further concentrated on the membranes (Figs. 4, 5, 7, and 8 A). Once shape changes cannot minimize the energy derived from elastic stress, lipid-packing defects occur in the inner leaflet, exposing the hydrophobic membrane interiors to drive hemifusion and fission (Inaoka and Yamazaki, 2007). We predict that by regulating the local concentration of the amphipathic N terminus through assembly, Sar1 can control constriction and fission. Fission induced by elastic stress is enhanced by the inclusion of ordered phase lipids that promote lipid packing (Inaoka and Yamazaki, 2007). Under these elastic-deficient conditions, we observed enhanced vesiculation morphology with the Sar1^{QTTG} mutant, which may further concentrate on membranes (Fig. 7 C).

Similar fission principals may apply in other cellular sites. As with Sar1, dynamin scaffolds restrict membrane constriction and fission, yet short transient assemblies promote fission (Pucadyil and Schmid, 2008). A hydrophobic residue in the unstructured loop of dynamin's PH domain is inserted in the membrane outer leaflet to regulate fission (Ramachandran et al., 2009). Dynamin assembly may regulate the local membrane imprint of this insertion to control fission. As with dynamin,

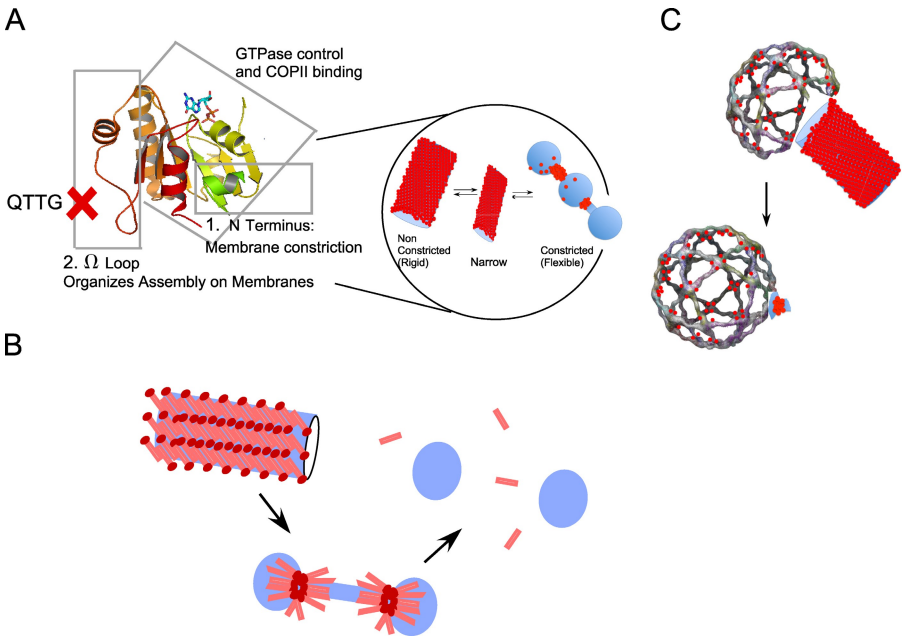

Figure 8. **Sar1 assemblies and membrane constriction.** (A) Sar1 utilizes the N terminus to constrict membranes and the Ω loop to organize Sar1 in scaffolds to regulate membrane constriction. (B) Based on an ADE model, the concentration of inserted Sar1 N terminus, which is controlled by assembly, can increase locally to induce membrane fission (pink bars, Sar1; red circles, N termini). (C) Sar1 (red circles) organization with relation to the assembled COPII cage. Nonconstricted tubules coated at the tip with COPII are visible in vitro (Aridor et al., 2001) and in vivo in fibroblasts derived from CLSD patients (Fromme et al., 2007). Vesicles connected through constricted necks are visible at ERES when fission is arrested with a GTPase-deficient Sar1 (Bielli et al., 2005). As depicted in the model, Sar1 is required in excess to support vesicle fission (Bielli et al., 2005).

GTP hydrolysis by Sar1 is required to release COPII vesicles. Future studies should examine the role of ADE in fission and determine whether the GTPase activity of Sar1 induces transient changes in the local concentration or orientation of the N terminus to further increase the area difference between the membrane leaflets and promote fission. Coat-induced changes in membrane tension may reduce the overall elasticity of the membrane to enhance vesicle release.

Regulation of Sar1 assembly

Membrane tethering was required to support the organization of Sar1 scaffolds on lipid tubules (Fig. 3). Tether-driven lateral tension imposes physical constraints that alter the diffusion properties of proteins and lipids and, therefore, protein–protein and protein–lipid interactions on and within the bilayer (Naumann et al., 2002). In semi-intact cells, Sar1 tubulates ER membranes to elongate a population of nonconstricted Sar1-coated rigid tubules (Fig. 4 D and Fig. S4; Aridor et al., 2001). In the absence of PI4P (either through PI4P sequestration of depletion of the phosphatidylinositol 4-kinases involved), the formation of Sar1-coated rigid tubules is prevented (Blumental-Perry et al., 2006; unpublished data), yet PI4P is not required for Sar1-induced scaffold formation on GUVs (Table S1). PI4P may function in cells to provide a binding site for membrane tethering at ERES akin to the artificial tethers provided in vitro for GUV attachment (Fig. 3). In support, we found that Sar1-coated rigid tubules were formed in siliconized chambers only with PI4P-containing GUVs in reactions supplemented with highly diluted cytosol (unpublished data). The identity and role of PI4P regulated tether factors remains to be defined.

Lipids regulate membrane constriction and fission

Diffusion barriers within the bilayer can concentrate and direct Sar1-induced membrane perturbation. GUVs that partition into Lo and Ld phases directed membrane tubulation exclusively to the Ld phase (Fig. 7 B). Similarly, ARF1 and COPI function on Ld lipid phases (Manneville et al., 2008). Unlike Golgi membranes on which COPI assembles, the ER has relatively low concentrations of cholesterol that preclude the formation of ordered lipid rafts (Allan, 1996). However, ER-sterols were shown to control COPII activities and ER export (Ridsdale et al., 2006; Runz et al., 2006). Depletion of sterols or inhibition of sterol synthesis reduce the mobility of membrane cargo proteins within the ER and inhibit the dynamic interactions of COPII subunits with ERES, leading to a strong inhibition of cargo capture and ER export. Thus, dynamic lipid microdomains can direct Sar1 activities and enhance lipid packing to support fission and ER exit.

Sar1 assembly and ER exit

Although $Sar1^{T158A}$ is deficient in its ability to support budding from the ER in defined reconstitution assays in vitro (Huang et al., 2001), the ER exit of GFP–VSV-G in vivo was insensitive to the expression of assembly-deficient $Sar1^{QTTG}$ that contains the T158A mutation (Fig. 6). Thus, functional deficiencies in $Sar1^{QTTG}$ were partially complemented by endogenous Sar1. The enhanced sensitivity of procollagen transport to the expression of $Sar1^{QTTG}$ suggests that the export of cargo that cannot be accommodated in COPII vesicles (60–80-nm diameter) presents more requirements to the COPII machinery. One possible explanation is that procollagen is exported from the ER in tubules that are Sar1 dependent yet COPII independent. However, this is unlikely, as similar differential inhibition of procollagen traffic is observed when cells are depleted of the COPII subunit Sec13 or in cranio lenticulo-sutural dysplasia (CLSD)–derived cells, which carry a point mutation in the COPII subunit Sec23a (Fromme et al., 2007; Townley et al., 2008). We propose an alternative model in which the regulation of membrane constriction at the vesicle neck by Sar1 affects carrier size and, thus, influences the ability to package cargo that is larger than COPII vesicles. When this regulation is perturbed through selective mutations that affect Sar1 organization (Figs. 4–6) or perturbed

regulation of Sar1–COPII interactions and GTPase activation as observed in CLSD (Fromme et al., 2007), the traffic of large cargoes is impaired. The selective loss of Sar1b expression or function leads to chylomicron (200–400 nm) accumulation in the ER in chylomicron retention disease (Jones et al., 2003). Our experiments were performed with a Sar1b homologue, and we did not detect significant differences when using Sar1a (unpublished data). Future studies should define how Sar1b–COPII interactions control Sar1b accumulation at the vesicle neck, thus regulating fission and vesicle size.

Materials and methods

Chemicals, plasmids, and proteins

DOPC, DOPS, dioleoyl phosphatidic acid, and PI4P were purchased from Avanti Polar Lipids, Inc. Cholesterol and Texas red DHPE were purchased from Sigma-Aldrich and Invitrogen, respectively. Alexa Fluor 488 maleimide was purchased from Invitrogen. Antibodies to COPII subunits were provided by W.E. Balch (The Scripps Research Institute, La Jolla, CA). Antibodies to Flag (M2) and collagen type I were obtained from Sigma-Aldrich and Millipore, respectively.

Mammalian expression vectors for Flag-tagged Sar1 and Sar1-GTP (H79G) were provided by S.I. Bannykh (Yale University, New Haven, CT). The 156QTTG/AAAA159 mutation was introduced in Sar1 proteins by site-directed mutagenesis using the oligonucleotides (forward) 5′-GAGAGATGTTTGGCTTATATGGGGCGGCAGCAGCAAAGGGCAGTGTGTCACTGAAGGAG-3′ and (reverse) 5′-CTCCTTCAGTGACACACTGCCCTTTGCTGCTGCCGCCCCATATAAGCCAAACATCTCTC-3′. Mutagenesis was verified by sequencing. GST-fused Sar1-H79G (Sar1-GTP) or Sar1 wt proteins were expressed in *Escherichia coli* and purified on glutathione Sepharose beads. Purified GST fusion proteins were digested with thrombin to remove the GST tag, and the cleaved proteins were subjected to further purification using ion exchange chromatography (Mono Q) as previously described (Barlowe et al., 1994). Purified proteins were dialyzed and stored at −80°C until use. Sar1-T39N (Sar1-GDP), Sar1-GTP, $Sar1^{QTTG}$, and GFP-Sar1-GTP were expressed in *E. coli* and purified as previously described (Rowe and Balch, 1995).

Fluorescently tagged Sar1 proteins

A GFP-tagged Sar1-GTP did not form rigid tubules (Fig. S3). Therefore, we tagged Sar1 with small fluorescent dyes for analysis. Random addition of primary amine-reactive dyes to Sar1 led to inactivation of the protein. Thus, we replaced the two cysteines of hamster Sar1a-GTP (H79G) with alanine residues (C102A and C178A) to prepare a cysteine-free protein (ΔC–Sar1-GTP) for targeted labeling. $Sar1\text{-}GTP^{C102A,C178A}$ was generated by two sequential site-directed mutagenesis reactions using quick change, and the cysteine-free mutant was expressed and purified for analysis. ΔC–Sar1-GTP was fully functional in coat assembly and the formation of rigid and flexible lipid tubules. We further added a cysteine at the C terminus (C199) of ΔC–Sar1-GTP using site-directed mutagenesis and prepared the protein for analysis. Surprisingly, the addition of this single-cysteine residue reduced the activities of Sar1, although the protein was still capable of forming rigid and flexible tubules when tested on GUVs, recruit COPII to membranes, and tubulate ERES. These results are in agreement with recent findings that demonstrate that tagging ARF1 at the C terminus modifies its basic activities (Jian et al., 2010). However, because the protein retained some functionality, Alexa Fluor 488 C6 maleimide (Invitrogen) was used to conjugate Alexa Fluor 488 to $Sar1\text{-}GTP^{H79G,\ C102A,C178A,CT99}$ according to the manufacturer's protocols.

Formation of GUVs

GUVs were electroformed as previously described (Mathivet et al., 1996). In brief, 5 µg of a lipid mixture dissolved in chloroform was deposited on an electrode coated with a thin transparent film of indium tin oxide. The electrode was placed in a desiccator and left for 2 h under vacuum. A spacer was placed on the electrode, and an appropriate buffer (see below) was injected through the spacer. An additional indium tin oxide electrode was placed on the spacer to assemble a chamber. The chamber was connected to a power supply and subjected to a low-frequency voltage (10 or 100 Hz) that was progressively increased from 0 to 1.2 V in 40 min for a total period of 220 min. To detach GUVs formed on the electrode, the chamber was subjected to additional low-frequency voltage (4 Hz and 1.4 V) for 10 min, and GUVs were recovered by gentle pipetting. GUVs were electroformed in low-salt buffer (25 mM Hepes-KOH, pH 7.2, and 1 mM $Mg(OAc)_2$), and GUVs composed of 54.5 mol% DOPC, 35 mol% DOPS, 10 mol% cholesterol, and 0.5 mol% Texas red DHPE were prepared in physiological salt buffer (25 mM Hepes-KOH, pH 7.2, 125 mM KOAc, and 1 mM $Mg(OAc)_2$).

Analysis of Sar1–GUV interactions

Incubations of GUVs with Sar1 proteins in a polypropylene tube were performed as follows: 5 µM Sar1 and 20 ng/µl GUVs were gently mixed in a buffer containing 25 mM Hepes-KOH, pH 7.2, 2.5 mM $Mg(OAc)_2$, 2.5 mM EDTA, and 2 mM GTP. Physiological salt buffer containing 25 mM Hepes-KOH, pH 7.2, 125 mM KOAc, 2.5 mM $Mg(OAc)_2$, 2.5 mM EDTA, and 2 mM GTP was used for GUVs composed of 54.5 mol% DOPC, 35 mol% DOPS, 10 mol% cholesterol, and 0.5 mol% Texas red DHPE. When indicated, 2 µM BSA was added to stabilize GUVs. Reaction mixes (10 µl final volume) were incubated at 32°C for 2 h in polypropylene tubes. At the end of incubation, an aliquot was gently injected into an observation chamber and analyzed using fluorescence microscopy.

Chamber formation and incubation of Sar1 with GUVs in chamber-based reactions

Incubation chambers were assembled by placing rectangular cover glasses onto glass slides using two double-sided tapes (3M; Scotch) as spacers (the gap between the spacers was 8 mm). For PLL-coated chambers and siliconized chambers, rectangular cover and slide glasses were coated with 0.01% PLL solution (Sigma-Aldrich) or siliconized with Sigmacote (Sigma-Aldrich) just before use. PLL-coated chamber was assembled with PLL-coated cover glass and siliconized glass slide, and the siliconized chamber was assembled with siliconized cover glass slides. A chamber built with uncoated cover glass slides was used for controls. 5 µM Sar1-GTP and 20 ng/µl GUVs were gently mixed in a buffer containing 25 mM Hepes-KOH, pH 7.2, 2.5 mM $Mg(OAc)_2$, 2.5 mM EDTA, and 2 mM GTP on ice, and immediately, 4.5 µl of the reaction was gently injected into the chambers. The chambers were incubated facedown at 32°C for 1 h in a humidified container placed in a humidified incubator. The resultant tubules were directly visualized in the chamber.

Microscopy

GUVs were visualized in reaction buffers at RT using a microscope (Microphot-FXL; Nikon) with a Plan Apo 100× 1.40 NA oil objective, and images were captured using a camera (Olympus) and MagnaFire software (version 2.0). When indicated, GUVs were similarly visualized using a confocal microscope (FV1000; Olympus) with a Plan Apo 60× 1.42 NA oil objective and captured using FluoView software (version 2.0; Olympus). Fixed cells were visualized using the confocal system (FV1000) in a similar manner. Images were prepared for presentation using Photoshop (CS3; Adobe) and Canvas X (ACD) with minimal processing.

Immunostaining of Sar1 on rigid tubules

GUVs were reacted with Sar1-GTP as described above. The samples were gently deposited on a cover glass or a PLL-coated cover glass and left for 5 min at RT. Excess cold methanol (−20°C) was gently added for 2 min at RT. Fixed samples were blocked with PBS containing 5% goat serum for 1 h at RT and stained with Sar1 antibodies.

Negative staining of tubules

GUVs (54.5 mol% DOPC, 35 mol% DOPS, 10 mol% cholesterol, and 0.5 mol% Texas red DHPE) were reacted with Sar1-GTP in a polypropylene tube as described above. At the end of incubation, the samples were absorbed onto formvar or carbon-coated copper EM grids (5–180 s), washed with 0.1 M Hepes, pH 7.4, stained with 1–2% uranyl acetate, blotted, and allowed to air dry for EM visualization. Samples were processed immediately after incubation or kept at 4°C before further processing. Sar1-induced tubulated GUVs were stable for several days. In Fig. 2 E, the sample was fixed with 2% paraformaldehyde for 10 min on ice. The sample was spotted on an EM grid and left to adhere overnight in a humidified chamber before staining as described above.

Quantification of Sar1-GTP–mediated rigid tubule formation

The mean number of fluorescent lipid particles indicative of lipid bilayers in 20 ng/µl GUVs solution in 1,000 μm^2 was determined in a fluorescence microscope using a 60× objective. Incubations were carried as described above, and the mean number of the formed rigid tubules in 1,000 μm^2 was counted using the 60× objective. Short tubules for which it was difficult to determine rigidity were not scored. The arbitrary units (AU) used were

defined as follows. AU = (mean number of rigid tubules/mean number of lipid signals indicative of lipid bilayers) × 100.

Coat assembly and morphological analysis in semi-intact cells

The recruitment of Sec23 to ER microsomes prepared from NRK cells was performed as previously described (Aridor et al., 1995; Pathre et al., 2003). In brief, microsomes were added to binding reactions containing rat liver cytosol and the indicated concentrations of Sar1 proteins (Aridor et al., 1995). Reactions were incubated at 32°C for 15 min and terminated by transfer to ice for 10 min. Membranes were salt washed and collected by centrifugation at 16,000 *g* for 15 min at 4°C, and membrane pellets were resuspended and resolved on SDS-PAGE 10.5% gels for Western blot analysis with Sec23-specific antibodies. The morphological analysis of coat assembly and tubulation of ERES in semi-intact NRK cells were performed as previously described (Aridor et al., 1995; Pathre et al., 2003; Blumental-Perry et al., 2006). In brief, NRK cells were permeabilized with 40 µg/ml digitonin in KHM buffer for 5 min on ice, washed with KHM, and incubated with transport cocktail (Aridor et al., 1995) in the absence (tubulation) or presence (coat assembly analysis) of rat liver cytosol at 32°C for 30 (coat assembly measurement) or 60 min (tubulation measurement). Cells were fixed in 4% formaldehyde in PBS for 15 min at RT for coat assembly analysis or with cold methanol (−20°C) for 1–2 min for tubulation analysis. (Pathre et al., 2003; Blumental-Perry et al., 2006)

Cells, viruses, and traffic assays

Viruses from the picornaviridae family, which use COPII to assemble replication complexes on ER membranes (Rust et al., 2001; Belov and Ehrenfeld, 2007), were used to infect Caco-2 cells as described previously (Coyne et al., 2004). The cells were plated in collagen-coated chamber slides (BD) at a density of 5×10^5 cells/well and cultured for 48–72 h. CVB3-RD (coxsackievirus B3 variant) was purified as described previously (Coyne and Bergelson, 2006). Experiments were performed with three to five plaque-forming units per cell. Monolayers were exposed to CVB3-RD in virus-binding buffer (Modified Eagle's Medium containing 20 mM Hepes) for 1 h at 4°C, washed, and incubated at 37°C for 7–9 h. Infected monolayers were fixed with ice-cold methanol/acetone (3:1) for 5 min at RT. Virus was detected with mouse antienterovirus VP1 (Ncl-Entero) antibody (Novocastra Laboratories), and Sar1 was detected with Sar1 antibodies.

MDCK cells stably expressing ts045–VSV-G–GFP (provided by A. Muesch, Albert Einstein College of Medicine, New York, NY) were maintained in DME, 10% FBS, 1% penicillin/streptomycin, 20 mM Hepes, pH 7.4, 2 mM L-glutamine, 20 ng/ml doxycycline at 37°C, and 5% CO_2. To analyze VSV-G transport, $0.9–1.0 \times 10^5$ cells were seeded onto coverslips in 6-well dishes the day before transfection. Cells were washed four times in 1× PBS and transfected with 0.6–0.8 µg Flag-Sar1a, Flag-Sar1a^{QTTG}, Flag-Sar1a-GTP, or Flag-Sar1a^{QTTG}-GTP using transfection reagent (Effectene) following standard protocol. Cells were grown in media lacking doxycycline at 37°C with 5% CO_2. At 8 h after transfection, cells were washed four times in 1× PBS, replaced with media containing 5 mM sodium butyrate, and grown at 40°C with 5% CO_2 overnight. At 24 h after transfection, cells were placed on ice, washed with ice-cold 1× PBS, and incubated in media containing 100 µg/ml cycloheximide at 32°C for the indicated times, fixed in 4% formaldehyde for 15 min at RT, washed with 1× PBS, and subjected to immunofluorescence.

Endogenous procollagen transport was analyzed in NIH3T3 cells. NIH3T3 cells were maintained in 1× DME, 10% FBS, 1% penicillin/streptomycin at 37°C, and 5% CO_2. For the analysis, $0.5–1.0 \times 10^5$ NIH3T3 cells were seeded onto acid-washed coverslips in 6-well dishes the day before transfection. Cells were transfected with Sar1-expressing plasmids as described above and grown at 37°C with 5% CO_2. At 48 h after transfection, cells were placed on ice, washed with ice-cold 1× PBS, and incubated in media containing 250 µM ascorbic acid, 1 mM ascorbate-2 phosphate, and 100 µg/ml cycloheximide at 37°C for the indicated times, fixed, and analyzed by immunofluorescence as described above.

Sar1 oligomerization analysis

Sar1 oligomerization analysis in the presence of extruded 400 µM LUVs prepared in low-salt buffer and cross-linking was performed essentially as described previously (Bielli et al., 2005) with the following modifications. Binding reactions were carried in low-salt buffer (15 mM Hepes, pH 7.2, 50 mM sorbitol, and 2.5 mM $Mg(OAc)_2$) supplemented with 2.5 mM EDTA, and 2 mM GTP or GDP as indicated, and for cross-linking analysis, BS^3 (Thermo Fisher Scientific) was used at 100 µM. At the end of the incubations, the reactions were centrifuged at 16,000 *g* for 15 min at 4°C to generate pellet and supernatant fractions. Sar1 oligomerization was analyzed by Western blotting using Sar1-specific antibodies.

Online supplemental material

Fig. S1 shows both widefield and confocal images of GUVs prepared in sucrose buffers in which tubulation is observed with Sar1-GTP (rigid and flexible) or Sar1^{QTTG}-GTP (flexible) but not with Sar1-GDP or Δ9-Sar1. Fig. S2 shows rigid tubule-like structures coated with endogenous Sar1 proteins that are formed in cells infected with CVB3 during replication complex assembly. Fig. S3 shows flexible tubules formed by a GFP-tagged Sar1-GTP, whereas the protein could not form rigid tubules. Fig. S4 shows the activity of a C-terminal–tagged Alexa Fluor 488 Sar1-GTP protein in COPII coat assembly at ERES and shows that Sar1 coats both flexible and rigid tubules on GUVs and at ERES. Fig. S5 compares the oligomerization pattern of Sar1-GTP and Sar1^{QTTG}-GTP using liposome membranes and cross-linking. Table S1 presents the tubulation outcome tested with GUVs made with various lipid compositions. Online supplemental material is available at http://www.jcb.org/cgi/content/full/jcb.201004132/DC1.

This work is dedicated to the memory of Dr. Anna Bielli.

This study is supported by National Institutes of Health (grants DK062318 and T32-DK061296 to M. Aridor and K.R. Long, respectively) and the Commonwealth of Pennsylvania SAP (grant 4100031302 to J.F. Conway).

Submitted: 27 April 2010
Accepted: 9 June 2010

References

Allan, D. 1996. Mapping the lipid distribution in the membranes of BHK cells (mini-review). *Mol. Membr. Biol.* 13:81–84. doi:10.3109/09687689609160580

Aridor, M., and K.N. Fish. 2009. Selective targeting of ER exit sites supports axon development. *Traffic.* 10:1669–1684. doi:10.1111/j.1600-0854.2009.00974.x

Aridor, M., S.I. Bannykh, T. Rowe, and W.E. Balch. 1995. Sequential coupling between COPII and COPI vesicle coats in endoplasmic reticulum to Golgi transport. *J. Cell Biol.* 131:875–893. doi:10.1083/jcb.131.4.875

Aridor, M., K.N. Fish, S. Bannykh, J. Weissman, T.H. Roberts, J. Lippincott-Schwartz, and W.E. Balch. 2001. The Sar1 GTPase coordinates biosynthetic cargo selection with endoplasmic reticulum export site assembly. *J. Cell Biol.* 152:213–229. doi:10.1083/jcb.152.1.213

Barlowe, C., L. Orci, T. Yeung, M. Hosobuchi, S. Hamamoto, N. Salama, M.F. Rexach, M. Ravazzola, M. Amherdt, and R. Schekman. 1994. COPII: a membrane coat formed by Sec proteins that drive vesicle budding from the endoplasmic reticulum. *Cell.* 77:895–907. doi:10.1016/0092-8674(94)90138-4

Bashkirov, P.V., S.A. Akimov, A.I. Evseev, S.L. Schmid, J. Zimmerberg, and V.A. Frolov. 2008. GTPase cycle of dynamin is coupled to membrane squeeze and release, leading to spontaneous fission. *Cell.* 135:1276–1286. doi:10.1016/j.cell.2008.11.028

Belov, G.A., and E. Ehrenfeld. 2007. Involvement of cellular membrane traffic proteins in poliovirus replication. *Cell Cycle.* 6:36–38.

Bi, X., R.A. Corpina, and J. Goldberg. 2002. Structure of the Sec23/24-Sar1 pre-budding complex of the COPII vesicle coat. *Nature.* 419:271–277. doi:10.1038/nature01040

Bi, X., J.D. Mancias, and J. Goldberg. 2007. Insights into COPII coat nucleation from the structure of Sec23.Sar1 complexed with the active fragment of Sec31. *Dev. Cell.* 13:635–645. doi:10.1016/j.devcel.2007.10.006

Bielli, A., C.J. Haney, G. Gabreski, S.C. Watkins, S.I. Bannykh, and M. Aridor. 2005. Regulation of Sar1 NH_2 terminus by GTP binding and hydrolysis promotes membrane deformation to control COPII vesicle fission. *J. Cell Biol.* 171:919–924. doi:10.1083/jcb.200509095

Blumental-Perry, A., C.J. Haney, K.M. Weixel, S.C. Watkins, O.A. Weisz, and M. Aridor. 2006. Phosphatidylinositol 4-phosphate formation at ER exit sites regulates ER export. *Dev. Cell.* 11:671–682. doi:10.1016/j.devcel.2006.09.001

Collins, C.A., and R.B. Vallee. 1987. Temperature-dependent reversible assembly of taxol-treated microtubules. *J. Cell Biol.* 105:2847–2854. doi:10.1083/jcb.105.6.2847

Coyne, C.B., and J.M. Bergelson. 2006. Virus-induced Abl and Fyn kinase signals permit coxsackievirus entry through epithelial tight junctions. *Cell.* 124:119–131. doi:10.1016/j.cell.2005.10.035

Coyne, C.B., T. Voelker, S.L. Pichla, and J.M. Bergelson. 2004. The coxsackievirus and adenovirus receptor interacts with the multi-PDZ domain protein-1 (MUPP-1) within the tight junction. *J. Biol. Chem.* 279:48079–48084. doi:10.1074/jbc.M409061200

de Silva, A.M., W.E. Balch, and A. Helenius. 1990. Quality control in the endoplasmic reticulum: folding and misfolding of vesicular stomatitis

virus G protein in cells and in vitro. *J. Cell Biol.* 111:857–866. doi:10.1083/jcb.111.3.857

Farsad, K., N. Ringstad, K. Takei, S.R. Floyd, K. Rose, and P. De Camilli. 2001. Generation of high curvature membranes mediated by direct endophilin bilayer interactions. *J. Cell Biol.* 155:193–200. doi:10.1083/jcb.200107075

Fath, S., J.D. Mancias, X. Bi, and J. Goldberg. 2007. Structure and organization of coat proteins in the COPII cage. *Cell.* 129:1325–1336. doi:10.1016/j.cell.2007.05.036

Forster, R., M. Weiss, T. Zimmermann, E.G. Reynaud, F. Verissimo, D.J. Stephens, and R. Pepperkok. 2006. Secretory cargo regulates the turnover of COPII subunits at single ER exit sites. *Curr. Biol.* 16:173–179. doi:10.1016/j.cub.2005.11.076

Fromme, J.C., M. Ravazzola, S. Hamamoto, M. Al-Balwi, W. Eyaid, S.A. Boyadjiev, P. Cosson, R. Schekman, and L. Orci. 2007. The genetic basis of a craniofacial disease provides insight into COPII coat assembly. *Dev. Cell.* 13:623–634. doi:10.1016/j.devcel.2007.10.005

Frost, A., R. Perera, A. Roux, K. Spasov, O. Destaing, E.H. Egelman, P. De Camilli, and V.M. Unger. 2008. Structural basis of membrane invagination by F-BAR domains. *Cell.* 132:807–817. doi:10.1016/j.cell.2007.12.041

Huang, M., J.T. Weissman, S. Beraud-Dufour, P. Luan, C. Wang, W. Chen, M. Aridor, I.A. Wilson, and W.E. Balch. 2001. Crystal structure of Sar1-GDP at 1.7 A resolution and the role of the NH_2 terminus in ER export. *J. Cell Biol.* 155:937–948. doi:10.1083/jcb.200106039

Inaoka, Y., and M. Yamazaki. 2007. Vesicle fission of giant unilamellar vesicles of liquid-ordered-phase membranes induced by amphiphiles with a single long hydrocarbon chain. *Langmuir.* 23:720–728. doi:10.1021/la062078k

Jian, X., M. Cavenagh, J.M. Gruschus, P.A. Randazzo, and R.A. Kahn. 2010. Modifications to the C-terminus of Arf1 alter cell functions and protein interactions. *Traffic.* 11:732–742. doi:10.1111/j.1600-0854.2010.01054.x

Jones, B., E.L. Jones, S.A. Bonney, H.N. Patel, A.R. Mensenkamp, S. Eichenbaum-Voline, M. Rudling, U. Myrdal, G. Annesi, S. Naik, et al. 2003. Mutations in a Sar1 GTPase of COPII vesicles are associated with lipid absorption disorders. *Nat. Genet.* 34:29–31. doi:10.1038/ng1145

Lee, M.C., E.A. Miller, J. Goldberg, L. Orci, and R. Schekman. 2004. Bi-directional protein transport between the ER and Golgi. *Annu. Rev. Cell Dev. Biol.* 20:87–123. doi:10.1146/annurev.cellbio.20.010403.105307

Lee, M.C., L. Orci, S. Hamamoto, E. Futai, M. Ravazzola, and R. Schekman. 2005. Sar1p N-terminal helix initiates membrane curvature and completes the fission of a COPII vesicle. *Cell.* 122:605–617. doi:10.1016/j.cell.2005.07.025

Manneville, J.B., J.F. Casella, E. Ambroggio, P. Gounon, J. Bertherat, P. Bassereau, J. Cartaud, B. Antonny, and B. Goud. 2008. COPI coat assembly occurs on liquid-disordered domains and the associated membrane deformations are limited by membrane tension. *Proc. Natl. Acad. Sci. USA.* 105:16946–16951. doi:10.1073/pnas.0807102105

Mathivet, L., S. Cribier, and P.F. Devaux. 1996. Shape change and physical properties of giant phospholipid vesicles prepared in the presence of an AC electric field. *Biophys. J.* 70:1112–1121. doi:10.1016/S0006-3495(96)79693-5

Matsuoka, K., L. Orci, M. Amherdt, S.Y. Bednarek, S. Hamamoto, R. Schekman, and T. Yeung. 1998. COPII-coated vesicle formation reconstituted with purified coat proteins and chemically defined liposomes. *Cell.* 93:263–275. doi:10.1016/S0092-8674(00)81577-9

McMahon, H.T., and J.L. Gallop. 2005. Membrane curvature and mechanisms of dynamic cell membrane remodelling. *Nature.* 438:590–596. doi:10.1038/nature04396

Mironov, A.A., A.A. Mironov Jr., G.V. Beznoussenko, A. Trucco, P. Lupetti, J.D. Smith, W.J. Geerts, A.J. Koster, K.N. Burger, M.E. Martone, et al. 2003. ER-to-Golgi carriers arise through direct en bloc protrusion and multistage maturation of specialized ER exit domains. *Dev. Cell.* 5:583–594. doi:10.1016/S1534-5807(03)00294-6

Naumann, C.A., O. Prucker, T. Lehmann, J. Rühe, W. Knoll, and C.W. Frank. 2002. The polymer-supported phospholipid bilayer: tethering as a new approach to substrate-membrane stabilization. *Biomacromolecules.* 3:27–35. doi:10.1021/bm0100211

Pathre, P., K. Shome, A. Blumental-Perry, A. Bielli, C.J. Haney, S. Alber, S.C. Watkins, G. Romero, and M. Aridor. 2003. Activation of phospholipase D by the small GTPase Sar1p is required to support COPII assembly and ER export. *EMBO J.* 22:4059–4069. doi:10.1093/emboj/cdg390

Pucadyil, T.J., and S.L. Schmid. 2008. Real-time visualization of dynamin-catalyzed membrane fission and vesicle release. *Cell.* 135:1263–1275. doi:10.1016/j.cell.2008.11.020

Ramachandran, R., T.J. Pucadyil, Y.W. Liu, S. Acharya, M. Leonard, V. Lukiyanchuk, and S.L. Schmid. 2009. Membrane insertion of the pleckstrin homology domain variable loop 1 is critical for dynamin-catalyzed vesicle scission. *Mol. Biol. Cell.* 20:4630–4639. doi:10.1091/mbc.E09-08-0683

Reynwar, B.J., G. Illya, V.A. Harmandaris, M.M. Müller, K. Kremer, and M. Deserno. 2007. Aggregation and vesiculation of membrane proteins by curvature-mediated interactions. *Nature.* 447:461–464. doi:10.1038/nature05840

Ridsdale, A., M. Denis, P.Y. Gougeon, J.K. Ngsee, J.F. Presley, and X. Zha. 2006. Cholesterol is required for efficient endoplasmic reticulum-to-Golgi transport of secretory membrane proteins. *Mol. Biol. Cell.* 17:1593–1605. doi:10.1091/mbc.E05-02-0100

Roux, A., D. Cuvelier, P. Nassoy, J. Prost, P. Bassereau, and B. Goud. 2005. Role of curvature and phase transition in lipid sorting and fission of membrane tubules. *EMBO J.* 24:1537–1545. doi:10.1038/sj.emboj.7600631

Rowe, T., and W.E. Balch. 1995. Expression and purification of mammalian Sarl. *Methods Enzymol.* 257:49–53. doi:10.1016/S0076-6879(95)57009-8

Runz, H., K. Miura, M. Weiss, and R. Pepperkok. 2006. Sterols regulate ER-export dynamics of secretory cargo protein ts-O45-G. *EMBO J.* 25:2953–2965. doi:10.1038/sj.emboj.7601205

Rust, R.C., L. Landmann, R. Gosert, B.L. Tang, W. Hong, H.P. Hauri, D. Egger, and K. Bienz. 2001. Cellular COPII proteins are involved in production of the vesicles that form the poliovirus replication complex. *J. Virol.* 75:9808–9818. doi:10.1128/JVI.75.20.9808-9818.2001

Shimoi, W., I. Ezawa, K. Nakamoto, S. Uesaki, G. Gabreski, M. Aridor, A. Yamamoto, M. Nagahama, M. Tagaya, and K. Tani. 2005. p125 is localized in endoplasmic reticulum exit sites and involved in their organization. *J. Biol. Chem.* 280:10141–10148. doi:10.1074/jbc.M409673200

Stagg, S.M., P. LaPointe, A. Razvi, C. Gürkan, C.S. Potter, B. Carragher, and W.E. Balch. 2008. Structural basis for cargo regulation of COPII coat assembly. *Cell.* 134:474–484. doi:10.1016/j.cell.2008.06.024

Starkuviene, V., and R. Pepperkok. 2007. Differential requirements for ts-O45-G and procollagen biosynthetic transport. *Traffic.* 8:1035–1051. doi:10.1111/j.1600-0854.2007.00582.x

Townley, A.K., Y. Feng, K. Schmidt, D.A. Carter, R. Porter, P. Verkade, and D.J. Stephens. 2008. Efficient coupling of Sec23-Sec24 to Sec13-Sec31 drives COPII-dependent collagen secretion and is essential for normal craniofacial development. *J. Cell Sci.* 121:3025–3034. doi:10.1242/jcs.031070

Wang, Q., M.V. Navarro, G. Peng, E. Molinelli, S.L. Goh, B.L. Judson, K.R. Rajashankar, and H. Sondermann. 2009. Molecular mechanism of membrane constriction and tubulation mediated by the F-BAR protein Pacsin/Syndapin. *Proc. Natl. Acad. Sci. USA.* 106:12700–12705. doi:10.1073/pnas.0902974106